Patterning of $Sc_{0.3}Al_{0.7}N$ Film for Piezoelectric MEMS Devices

Zhan Jiang Quek
*Institute of Microelectronics (IME), Agency for Science, Technology and Research (A*Star)*
Republic of Singapore
quek_zhan_jiang@ime.a-star.edu.sg

Minghua Li
*Institute of Microelectronics (IME), Agency for Science, Technology and Research (A*Star)*
Republic of Singapore
li_minghua@ime.a-star.edu.sg

Yan Hong
*Institute of Microelectronics (IME), Agency for Science, Technology and Research (A*Star)*
Republic of Singapore
hong_yan@ime.a-star.edu.sg

Yijun Lim
*Institute of Microelectronics (IME), Agency for Science, Technology and Research (A*Star)*
Republic of Singapore
lim_yijun@ime.a-star.edu.sg

Huamao Lin
*Institute of Microelectronics (IME), Agency for Science, Technology and Research (A*Star)*
Republic of Singapore
lin_huamao@ime.a-star.edu.sg

Abstract**—Piezoelectric coefficient in $Sc_xAl_{1-x}N$ was reported to increase as scandium-doping *x* increases up to 43%. However, the patterning of $Sc_{0.3}Al_{0.7}N$ film for the fabrication of piezoelectric micro-electromechanical systems (MEMS) devices poses challenges such as low etch rate, uncontrollable sidewall profile, micro-trenching, and significant bottom molybdenum (Mo) electrode loss. In this work, engineering of the sidewall profile by etch byproduct redeposition through plasma etch parameters and development of $Sc_xAl_{1-x}N$ etch with a soft landing on the bottom Mo electrode was investigated. Post-etch analysis on the exposed $Sc_{0.3}Al_{0.7}N$ sidewall was also performed to validate any presence of conducting residues and surface oxidation.**

Keywords—Piezoelectric $Sc_{0.3}Al_{0.7}N$, dry plasma etching

I. Introduction

Scandium-doped Aluminum Nitride ($Sc_xAl_{1-x}N$) has attractive piezoelectric, ferroelectric, pyroelectric, and optoelectrical properties which are desirable for various devices such as radio frequency filters, piezoelectric micromachined ultrasonic transducers, ferroelectric random-access memory array and waveguides [1-3]. The piezoelectric coefficient increases as the scandium-doping concentration increases up to 43% [4]. An increase in scandium-doping concentration beyond 43% results in the degradation of piezoelectric response due to the transition from the hexagonal wurtzite crystal structure to the cubic rock-crystal salt structure [5].

In AlN film, the nitrogen atoms and aluminum atoms are tetrahedrally coordinated to form the hexagonal wurtzite crystal structure. During the growth of $Sc_xAl_{1-x}N$ film, substitutional doping of scandium for aluminum atom occurs and were found to coordinate in a similar manner with nitrogen atoms while maintaining the hexagonal wurtzite structure. As the scandium-doping concentration increases, the stoichiometric amount of Sc-N bonding increases. Sc-N bond energy (13.35 eV) is higher than a typical Al-N bond (11.52 eV) which leads to higher hardness in $Sc_xAl_{1-x}N$ film at higher scandium-doping [6]. In the dry plasma etching of highly doped $Sc_xAl_{1-x}N$ film, higher physical bombardment is required to break the Sc-N bonds and further chemical reaction to form the desired pattern.

The patterning of $Sc_xAl_{1-x}N$ film can be performed using either dry plasma etching or wet chemical etching. Anisotropic dry plasma etching under a photoresist mask without lateral etching is preferred. In our previous work in [7], the sidewall profile optimization was performed on $Sc_{0.2}Al_{0.8}N$ film. However, when the same etching regime was employed on $Sc_{0.3}Al_{0.7}N$, the results were undesirable. The formation of duo-step, micro-trenching, significant bottom molybdenum (Mo) electrode loss, and reduction in etch rate poses challenges in the integration of $Sc_{0.3}Al_{0.7}N$-based piezoelectric micro-electromechanical systems (MEMS) devices. In this work, sidewall profile optimization for $Sc_{0.3}Al_{0.7}N$ and the development of a soft landing etch with minimal Mo loss were presented.

II. Experimental

500nm silicon oxide was deposited on a 200mm Si wafer using a plasma-enhanced chemical vapor deposition (PECVD) system. Subsequently, 20nm AlN seed/ 200nm Mo/ 1000nm $Sc_{0.3}Al_{0.7}N$/ 100nm Mo stack film was deposited using the physical vapor deposition (PVD) system without vacuum break and patterned using *i*-line lithography. A chlorine-based plasma was used to etch the top Mo electrode landing on $Sc_{0.3}Al_{0.7}N$ film. The $Sc_{0.3}Al_{0.7}N$ film etching experiments were carried out using Ar/Cl_2 plasma chemistry. Post-etch photoresist strip was carried out in oxygen plasma and polymer byproduct cleaning using NE-14. The wafers were imaged and characterized using a defect-review scanning electron microscope (DRSEM), cross-sectional scanning electron microscope (cross-SEM), and transmission electron microscopy (TEM).

III. Results and Discussion

A. ScAlN etch optimisation

Using the optimised etching regime for $Sc_{0.2}Al_{0.8}N$ from our previously reported work in [7] to etch $Sc_{0.3}Al_{0.7}N$ film, there was a difference in the sidewall profile as shown in **Fig. 1**. During the etch of $Sc_xAl_{1-x}N$ film in chlorine-based chemistry, etch byproducts such as $ScCl_3$, $AlCl_3$, and Al_2Cl_6 will be generated [8]. The redeposition of $ScCl_3$ with low vapor pressure and boiling point was expected [9]. Volatile $AlCl_3$ and Al_2Cl_6 can be easily vaporized and removed from the etching system. Due to the change in elemental composition when etching $Sc_{0.3}Al_{0.7}N$, the proportion of byproduct formation is affected which resulted in a change in the sidewall profile.

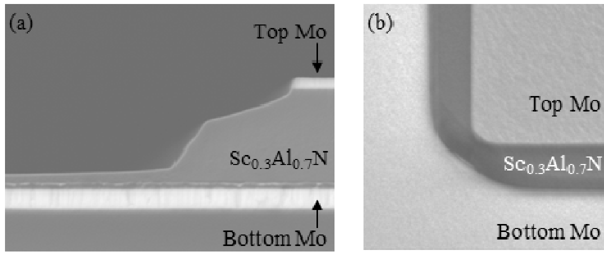

Fig 1. (a) Cross-section SEM inspection and (b) defect-review SEM image of etched $Sc_{0.3}Al_{0.7}N$ before process optimisation.

In the generation of a tapered sidewall profile, etch byproduct redeposition method was proposed in this work. The redeposited byproduct on the sidewall function as a micro-masking that covers the $Sc_{0.3}Al_{0.7}N$ and hinders further etching. During dry plasma etching, the wafer temperature will gradually increase due to the physical bombardment and chemical reaction occurring on the wafer surface. Although helium gas was applied on the wafer's backside as a cooling mechanism, the long etching time for highly doped $Sc_xAl_{1-x}N$ film could cause the wafer to heat up over time. When the wafer temperature increases, the sticking coefficient of the etch byproduct to the sidewall decrease. The bottom sidewall profile tends to become relatively vertical due to the reduced sidewall redeposition.

Modification of the etching parameters to engineer the sidewall redeposition can effectively create different types of sidewall profiles as shown in **Fig. 2** for different applications. A convex (**Fig. 2a**) and concave (**Fig. 2c**) profile can be achieved in a physical and chemically etching condition respectively. Optimization of the synergistic impact of both physical and chemical aspects of dry plasma etching results in a uniform profile (**Fig 2b**).

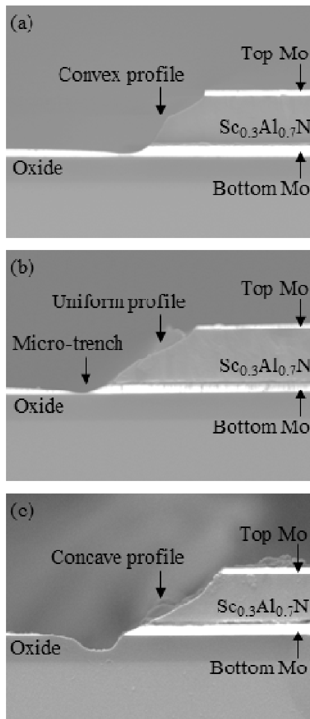

Fig 2. Different types of angles are achieved from different etching processes. Cross-SEM of (a) convex profile in a more physical etching process, (b) relatively uniform profile from optimised process and (c) concave profile in a more chemical etching process.

B. $Sc_xAl_{1-x}N$ etch with a soft landing on Mo electrode

As demonstrated in **Fig. 2**, we report the issue of micro-trenching in $Sc_{0.3}Al_{0.7}N$ etching. Formation of micro-trenching during the etching of dielectric materials is a common challenge due to the tendency for dielectric material to charge on the sidewall. The attraction of charged species toward the sidewall leads to an enhancement in the local etch rate and results in the formation of a micro-trench. In the case of $Sc_{0.3}Al_{0.7}N$ etching, it was hypothesized that the charging of $Sc_{0.3}Al_{0.7}N$ and redeposited etch byproduct led to the formation of micro-trenching.

$Sc_{0.3}Al_{0.7}N$ etching in reactive chlorine-based plasma require physical etching power due to the stronger Sc-N bonding. Metal electrodes can also be etched in similar etching conditions, which leads to the challenge of achieving high selective etching of $Sc_{0.3}Al_{0.7}N$ against Mo. As shown in **Fig. 2**, more Mo electrode loss was seen at the footing of the Mo/ScAlN pattern due to micro-trenching and poor selectivity against Mo. In the worst-case scenario, Mo can be completely etched away resulting in device failure due to disconnection of the bottom Mo electrode.

To improve device fabrication reliability, the development of selective etch or reduction of micro-trenching formation is essential. In this work, we proposed a soft landing etch of $Sc_{0.3}Al_{0.7}N$. By reducing the physical sputtering etching power, the etch rates of both $Sc_{0.3}Al_{0.7}N$ and Mo can be reduced, giving more process windows for stopping on Mo. With the implementation of a second soft landing etch of $Sc_{0.3}Al_{0.7}N$, stopping on the bottom Mo electrode, a significant reduction in bottom Mo loss was achieved as shown in **Fig. 3a**.

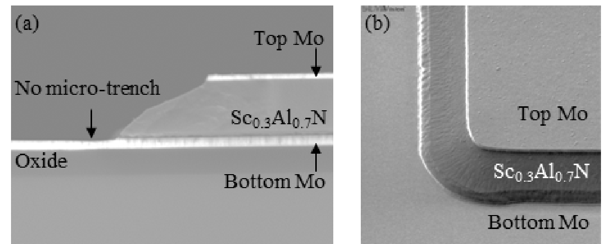

Fig 3. (a) Cross-section SEM inspection and (b) defect-review SEM image of etched $Sc_{0.3}Al_{0.7}N$ after process optimization and implementation of second soft landing step.

C. Post etch TEM sidewall analysis

In this work, the tapered profile was obtained through the etch byproduct redeposition that acts as a micro-mask. Further investigations were performed to verify if the wet polymer cleaning step is effective to remove the redeposited etch byproduct. Any presence of conductive residues on the sidewall that connects the top and bottom electrodes will lead to device failure. Polymers also may create adhesion issues in the following PECVD deposition in the integration flow. DRSEM top-down (**Fig 3b**) and TEM analysis (**Fig 4b**) on the sidewall suggests that the sidewall is clean without any metallic material. It indicates that the post-etch photoresist removal and wet polymer are efficient.

It was observed through high-resolution TEM analysis on the etched sidewall that the film remains crystalline after the processes. Also, there is no surface oxidation on the exposed ScAlN sidewall, as illustrated in **Fig. 4c**. This suggests that

this etching regime is suitable for the fabrication of a piezoelectric MEMS device.

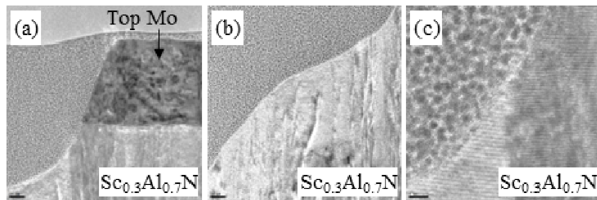

Fig 4. TEM on (a) top Mo electrode and (b) etched $Sc_{0.3}Al_{0.7}N$ sidewall. (c) High-resolution TEM on etched $Sc_{0.3}Al_{0.7}N$ sidewall

IV. CONCLUSION

In conclusion, the challenge in dry plasma etching of $Sc_{0.3}Al_{0.7}N$ as compared to lower scandium-doped $Sc_xAl_{1-x}N$ films was reported. In this paper, profile sidewall optimization through the engineering of etch byproduct generation and development of soft landing etch of $Sc_{0.3}Al_{0.7}N$ etch stopping on the bottom Mo electrode to mitigate the issues with micro-trenching was presented. Post-etch analysis suggests that the wet polymer cleaning was effective using NE-14 and no surface oxidation on the exposed $Sc_{0.3}Al_{0.7}N$ sidewall.

$Sc_xAl_{1-x}N$ has demonstrated great potential in the application of various piezoelectric MEMS devices. The current progress in etching process technology for $Sc_{0.3}Al_{0.7}N$ film with higher scandium-doping AlN films is expected to drive further advancement with more emerging piezoelectric applications.

ACKNOWLEDGMENT *(Heading 5)*

This work was supported by the Science and Engineering Research Council of A*STAR (Agency for Science, Technology and Research) Singapore, under Grant No. A20G9b0135.

REFERENCES

[1] Y. Zhang et al., "3D monolithic integration of ScAlN-based GHz MEMS acoustic filters on 200mm RFSOI wafer," in 2022 International Electron Devices Meeting (IEDM), 2022: IEEE, pp. 16.2. 1-16.2. 4.

[2] S. Fichtner, N. Wolff, F. Lofink, L. Kienle, and B. Wagner, "AlScN: A III-V semiconductor based ferroelectric," Journal of Applied Physics, vol. 125, no. 11, 2019.

[3] X. Zhang et al., "Aluminum scandium nitride waveguide in the near-infrared," in 13th International Photonics and OptoElectronics Meetings (POEM 2021), 2022, vol. 12154: SPIE, pp. 78-85.

[4] M. Akiyama, T. Kamohara, K. Kano, A. Teshigahara, Y. Takeuchi, and N. Kawahara, "Enhancement of piezoelectric response in scandium aluminum nitride alloy thin films prepared by dual reactive cosputtering," Advanced Materials, vol. 21, no. 5, pp. 593-596, 2009.

[5] S. Satoh, K. Ohtaka, T. Shimatsu, and S. Tanaka, "Crystal structure deformation and phase transition of AlScN thin films in whole Sc concentration range," Journal of Applied Physics, vol. 132, no. 2, 2022.

[6] X. Wang, W. Lin, X. Yun, Q. Zha, H. Li, and B. Zhang, "Research of etching process of Al0. 8Sc0. 2N based on ICP etching equipment," in 2021 5th IEEE Electron Devices Technology & Manufacturing Conference (EDTM), 2021: IEEE, pp. 1-3.

[7] Z. J. Quek, H. Lin, Y. F. Tsang, and B. C. Rao, "Tunable Etch Profile for Scandium Doped Aluminum Nitride Piezoelectric Film," in 2022 IEEE 24th Electronics Packaging Technology Conference (EPTC), 2022: IEEE, pp. 594-597.

[8] Z. Luo, S. Shao, and T. Wu, "Optimization of AlN and AlScN film ICP etching," in 2021 IEEE 34th International Conference on Micro Electro Mechanical Systems (MEMS), 2021: IEEE, pp. 638-641.

[9] M. T. Hardy, B. P. Downey, D. J. Meyer, N. Nepal, D. F. Storm, and D. S. Katzer, "Epitaxial ScAlN etch-stop layers grown by molecular beam epitaxy for selective etching of AlN and GaN," IEEE Transactions on Semiconductor Manufacturing, vol. 30, no. 4, pp. 475-479, 2017.